Carrier accumulation near electrodes in ferroelectric films due to polarization boundary conditions

I. B. Misirlioglu and M. Yildiz

Articles you may be interested in

Electrical and photoelectrical characterization of undoped and S-doped nanocrystalline diamond films
J. Appl. Phys. **103**, 084905 (2008); 10.1063/1.2908884

Polarization reversal and capacitance-voltage characteristic of epitaxial Pb (Zr , Ti) O 3 layers
Appl. Phys. Lett. **86**, 192902 (2005); 10.1063/1.1926403

Schottky emission at the metal polymer interface and its effecton the polarization switching of ferroelectric poly(vinylidenefluoride-trifluoroethylene) copolymer thin films
Appl. Phys. Lett. **85**, 1719 (2004); 10.1063/1.1786364

Competition between ferroelectric and semiconductor properties in Pb (Zr 0.65 Ti 0.35) O 3 thin films deposited by sol–gel
J. Appl. Phys. **93**, 4776 (2003); 10.1063/1.1562009

Leakage current behavior of SrBi 2 Ta 2 O 9 ferroelectric thin films on different bottom electrodes
J. Appl. Phys. **92**, 6160 (2002); 10.1063/1.1515104

Carrier accumulation near electrodes in ferroelectric films due to polarization boundary conditions

I. B. Misirlioglu[a)] and M. Yildiz
Faculty of Engineering and Natural Sciences, Sabanci University, Tuzla/Orhanli, 34956 Istanbul, Turkey

We study the effect of surface polarization on the distribution of free carriers in a wide bandgap semiconductor ferroelectric (FE) film using a thermodynamic approach. We show that free carriers, namely, holes and electrons from ionizable impurities or atomic vacancies can accumulate near the film-electrode interface, if FE polarization profile has a very steep change near the surface that is specified by the extrapolation length. Such an outcome is just the opposite of what happens in a Schottky junction in a partially or fully depleted film. This is also an entirely different effect than what has been often studied in similar structures, where the work function and screening length of the electrode metal determines the electronic character of the interface. Even for low-to-moderate densities of ionizable defects with states within the bandgap close to the band edges, high densities of carriers can localize close to the electrodes in a single domain state FE film when above a critical thickness. For very low densities of such ionizable defects, short extrapolation lengths cause electrical domain formation with minimal carrier accumulation because of the already weak depolarizing fields. This is also true for films below a critical thickness with low-to-moderate densities of ionizable impurities, i.e., electrical domains get stabilized regardless of defect density. The implications of our findings for polarization controlled Schottky to Ohmic-like transition of an interface and experimental results are discussed. It is also found that interfaces of an *n*-type FE heterostructure can behave like a *p*-type depending on the barrier heights and impurity density. We conclude that, for low-to-moderate ionizable impurity densities, it is the rate of change of polarization at the interface with position rather than solely its presence that leads to carrier accumulation and that both interfaces can become Ohmic-like with opposite signs of carriers. © 2014 AIP Publishing LLC. [http://dx.doi.org/10.1063/1.4886576]

I. INTRODUCTION

Distribution of charge carriers in ferroelectric (FE) heterostructures remains an important factor in device design tailoring the polar state. FE oxide perovskites are the most interesting structures in this regard and are also wide bandgap semiconductors. Use of these materials as gate-control layers and data retention components in high-density memory architectures is an on-going interest.[1–6] The presence of FE polarization alters the classical characteristics of film-electrode junctions in an otherwise linear dielectric semiconductor, making polarization manipulation of carriers possible[6–9] but at the expense of potential leakage currents.[10–15] For this very reason, electrical and polarization boundary conditions (BCs) at the film-electrode interface become crucially important parameters that determine the functionality of these systems almost regardless of film thickness. Significant number of studies have been devoted to clarifying the effect of semiconducting properties of FEs on their hystereses, capacitance-voltage, and current-voltage behavior,[4,16,2,3,10,11,13,17–21] where the only difference is apparently the consideration of an additional built-in field due to polarization inserted to the equations next to the built-in field due to the Schottky character of the

junction.[10,11,13,22] A number of other works adopt thermodynamic approaches coupled with electrostatics and semiconductor equations for a given FE-electrode couple.[23–30] While the importance of electrical and polarization BCs on properties of FE films is very well anticipated, only a handful of relatively recent studies have seriously tried to address their impact on the properties.[27,31–38] Given the great importance of the BCs and the theoretically proven sensitivity of FE films to interface characteristics in sandwich type FE thin film capacitor structures, observing hysteresis loops and butterfly type C-V curves in these systems is a routine practice but is also quite contraversial. The reason behind this thought is that the electrodes used to contact the FE film often have finite screening lengths[39,40] and that thermodynamic analysis has shown the ultimate stability of multidomain (MD) state in these systems.[41,42] Assuming at the moment that the electrodes behave as nearly ideal, another parameter coming into play is the "strength" of the ferroelectricity near the interfaces: Keeping in mind that FE ordering is a result of long range Coulomb interactions,[43,44] termination of the polar lattice, despite the presence of electrodes providing image dipoles, at the surface can be expected to suppress ferroelectricity with respect to the bulk and also smear the anomalies.[21,45] Such an effect is introduced into the thermodynamic calculations via the well-known polarization BCs in a form, where a so-called extrapolation length acts to suppress ferroelectricity at the interface when positive or vice

---

a)Author to whom correspondence should be addressed. Electronic mail: burc@sabanciuniv.edu

versa. Particularly, in Ref. 36, the tendency of surface polarization to go to zero was shown, pointing to very short extrapolation lengths. Glinchuk *et al.* pointed out to the importance of the extrapolation length on the magnitude of the depolarizing fields in a ferroelectric slab.[38] In an older paper, Kretschmer and Binder have shown the importance of polarization BCs on the stability of the single domain (SD) state in a "uniaxial" FE.[46] In a FE with weaker anisotropy, where polarization rotation is possible, strong suppression of the FE ordering near the interface can trigger domain formation to localize the depolarizing fields near the interface as mentioned in more recent works.[41,42]

Here, we study the effect of polarization gradients near the interfaces imposed by the extrapolation length on carrier distribution in a FE semiconductor. A short extrapolation length corresponds to a "weaker ferroelectricity" and that the system is certainly not in global minima near the interface. Schottky type interfaces in dielectric semiconductors have carrier depletion near the interfaces and this is also true for FE layers with interfaces having the same Curie point (T_C) as the bulk. We demonstrate that this picture can entirely change if the surface has a lower Curie point than the bulk, leading to polarization gradients near the interface. If these gradients are too steep, i.e., strong suppression of ferroelectricity near the interfaces is the case, electrical domains can form. Note that this is not related to the finite screening effect of electrodes, which is often claimed to trigger electrical domain formation in thin films. Just as interesting, in relatively thick films (>40 nm in this work) another type of behavior takes place where low-to-moderate amounts of ionizable (donating electrons to the conduction band or accepting electrons form the valence band) impurity densities charge can lead to accumulation of free carriers near the electrodes that apparently compensates the electric fields due to abrupt polarization gradients near the interfaces. For such films, SD state is possible unlike in the case of "ideal insulating dielectric" assumption because the latter always ends up with domains for steep polarization gradients at the surfaces due to short extrapolation lengths. However, such interfaces can behave as Ohmic-like and lead to potential leakage currents. In all cases, when multidomain state occurs, negligible carrier accumulation is observed near the interfaces and the films are in fully depleted state in the range of thicknesses considered here. We emphasize the dramatic effect of how polarization termination at a FE-metal interface impacts the Schottky character of a FE film with *n*-type ionizable impurities having a work function lower than that of the metal electrode: carrier depletion behavior is reversed whereby the depletion zone dominated by ionized impurities moves to the center of the FE film, just the opposite of what happens in a Schottky interface. This may or may not be classified as an Ohmic one as an Ohmic junction requires low barrier heights, hence we name it Ohmic-like in the rest of the paper. Such an outcome of our work could be important in evaluating the leakage mechanisms, in particular, capacitance and hystereses behavior. We also find that, for low-to-moderate impurity densities, it is the rate of change of polarization near the interface that determines whether the interface can behave as a Schottky or Ohmic-

like in addition to the sign of polarization with respect to the electrodes. Presence of a nearly homogeneous polarization throughout the thickness of the film does not lead to a varying electronic character of the top and bottom electrode interfaces and the regular symmetrical Schottky interfaces at top and bottom electrodes persist at zero bias. We also demonstrate that in the case of very high impurity densities, the carrier distribution becomes relatively insensitive to the extrapolation length and we comment on this in the light of a recently analyzed case in literature.

II. THEORY AND METHODOLOGY

The schematic of the capacitor film system we study is in Figure 1. A grid in the *x-z* plane is constructed as $h = m \times u$ and $p = 200 \times u$ with u being the unitcell distance and is approximately the unitcell length of the FE in the cubic state, m is the number of unitcells along thickness, h. We take PbZr$_{0.3}$Ti$_{0.7}$O$_3$ (PZT) grown epitaxially on SrTiO$_3$ (ST) substrate with thin coherent Pt electrodes as an example: this system has a lattice misfit of around -1% (compression) and can sustain interfacial coherency up to around 40 nm of thickness followed by a very large dislocation period that has a minimal impact of strain relaxation up to around 80 nm of thickness. The electrodes are considered to be also coherent with the ST substrate.

A semiconductor dielectric with impurities that donate electrons to the conduction band will have a total charge density, ρ, of

$$\rho(r) = N_D^+(r) + n^-(r) + p^+(r), \quad (1)$$

where the individual terms on the right handside are

$$N_D^+ = N_D(1 + g_D \exp[q(E_D - E_F - \phi)/kT])^{-1}, \quad (2a)$$

$$n^- = N_C(1 + \exp[q(E_C - E_F - \phi)/kT])^{-1}, \quad (2b)$$

$$p^+ = N_V(1 - [1 + \exp(q(E_V - E_F - \phi)/kT)]^{-1}). \quad (2c)$$
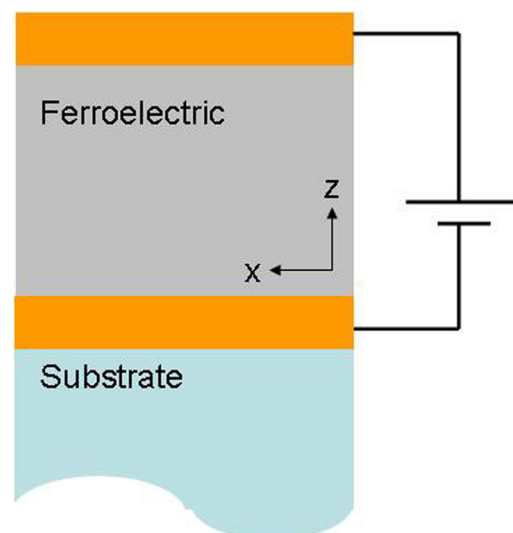
FIG. 1. Schematic of the capacitor thin film structure studied in this work.

TABLE I. Constants used in computing the semiconducting parameters (Vacuum level is reference and taken as zero).

E_F	E_D	E_V	E_C	φ (Pt)	N_C	N_V
−5.1 eV (intrinsic) (for when with impurities, please check Figure 2)	−4.0 eV	−6.6 eV	−3.6 eV	−5.5 eV	10^{24}	10^{24}

In Eq. (2), N_D^+ is the ionized impurity density, n^- is the electron density, p^+ is the hole density, N_C is the effective density of states at the bottom of the conduction band, N_V is the effective density of states at the top of the valence band, E_C is the energy of an electron at the bottom of the conduction band, E_V is the energy of an electron at the top of the valence band, E_F is the Fermi level, ϕ is the local electrostatic potential. Before going onto any calculation, one needs to know the E_F of the semiconductor for a given impurity density, N_D, varying as a function of coordinate r with an ionization energy $E_C - E_D$ (taken with respect to the bottom of the conduction band) from the charge neutrality condition

$$\int dV \rho(r) = 0. \tag{3}$$

The integration over the volume can be replaced with summation over the coordinates in a discrete grid system that is used in the current work yielding

$$\sum_N \rho(x, y) = 0. \tag{4}$$

For a homogeneous impurity distribution and infinite semiconductor with equal amounts of positive and negative charges, coordinates will not matter for charge neutrality condition. In (4), the summation runs over all sites, where N is the total number of sites and ρ is a function of coordinates x and z. Using the parameters given in Table I, varying the homogeneous impurity density and following a graphical solution method, we get the plot in Figure 2 for the E_F as a function of temperature for the impurity densities of interest in this study.

Knowing E_F of the FE semiconductor, we have to satisfy the Poission Equation in our film given as
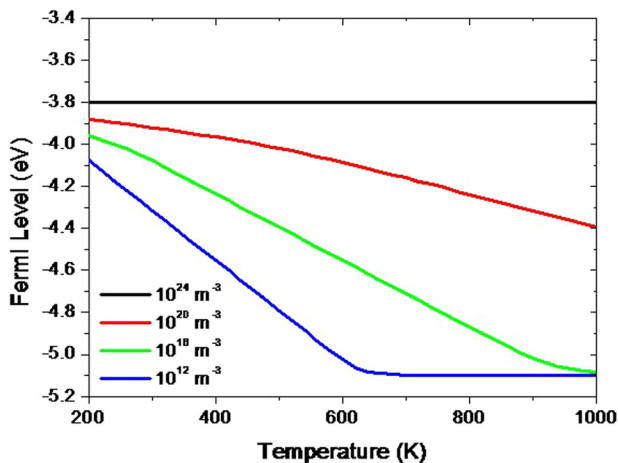
FIG. 2. Fermi level computed as a function temperature.

$$\nabla \cdot \vec{D} = \rho, \tag{5}$$

where $\vec{D} = D_x \vec{e}_x + D_z \vec{e}_z$, $D_x = \varepsilon_o \varepsilon_b E_x + P_x$, and $D_z = \varepsilon_o \varepsilon_b E_z + P_z$. Here, $\vec{D}$ is the dielectric displacement vector, ε_o is the permittivity of vacuum, and ε_b is the background dielectric constant (7 in this work[47,48]), E_x and E_z are, respectively, the $x-$ and $z-$ components of the electric field vector $\vec{E}$ determined from $E_x = -\partial \phi / \partial x$ to $E_z = -\partial \phi / \partial z$, P_x and P_z are the FE polarization components along x and z, respectively. The polarization terms in the dielectric displacement vector make the difference between a regular dielectric semiconductor and a FE one. Polarization components satisfy the Landau-Ginzburg equations of state written as

$$2\alpha_3^m P_z + 4\alpha_{13}^m P_z P_x^2 + 4\alpha_{33}^m P_z^3 + 6\alpha_{111} P_z^5$$
$$+ \alpha_{112}\left(4P_z P_x^4 + 8P_z^3 P_x^2\right) + 2\alpha_{123} P_z P_x^4$$
$$- G\left(\frac{\partial^2 P_z}{\partial z^2} + \frac{\partial^2 P_z}{\partial x^2}\right) = -\frac{\partial \phi}{\partial z}, \tag{6a}$$

$$2\alpha_1^m P_x + 2(2\alpha_{11}^m + \alpha_{12}^m)P_x^3 + 2\alpha_{13}^m P_x P_z^2 + 6\alpha_{111} P_x^5$$
$$+ 2\alpha_{112}\left[3P_x^5 + 3P_x^3 P_z^2 + P_x P_z^4\right] + 2\alpha_{123} P_x^3 P_z^2$$
$$- G\left(\frac{\partial^2 P_x}{\partial z^2} + \frac{\partial^2 P_x}{\partial x^2}\right) = -\frac{\partial \phi}{\partial x}, \tag{6b}$$

where α_3^m, α_{13}^m, α_{33}^m, α_1^m, α_{11}^m, and α_{12}^m are the renormalized dielectric stiffness coefficients in SI units with α_1^m and α_3^m containing the strain renormalization as $\alpha_1^m = \alpha(T - T_C) - u_{ij}^M (Q_{11} + Q_{12})/(S_{11} + S_{12})$ and $\alpha_3^m = \alpha(T - T_C) - 2u_{ij}^M Q_{12}/(S_{11} + S_{12})$, where $\alpha = (2\varepsilon_0 C)^{-1}$, α_{12}^m and α_{33}^m contain the clamping effect of the film, while α_{111}, α_{112}, and α_{123} are the dielectric stiffness coefficients in the bulk and can be found for various compositions of Pb, Zr, and TiO$_3$ in Ref. 49, u_{ij}^M is the misfit strain tensor for a cubic structure. G is the gradient energy coefficient and is assumed to be isotropic for convenience, with a value of 6×10^{-10} m^3/F.[42] We solve Eqs. (4), (5), and (7) spontaneously in a numerical iterative scheme on a discrete grid with the top-bottom interface polarization BCs given as

$$\lambda \frac{\partial P_x}{\partial x} - P_x = 0 \big|_{z=0,h} \quad \text{and} \quad \lambda \frac{\partial P_z}{\partial z} - P_z = 0 \big|_{z=0,h} \tag{7}$$

with h being the film thickness, λ is the extrapolation length determining the extent of change of polarization along the film normal at the interface and is a parameter implying how strongly Ferroelectricity is suppressed near the interfaces. As we shall see later, this parameter has a dramatic impact on the depletion behavior of near the interfaces. Periodic BCs are employed along the film plane both for polarization and electrostatic potential. The BCs for electrostatic potential are specified at the FE-electrode interfaces as the difference

between the E_F of the FE and the electrode (namely, the barrier height), where $\phi = \varphi \pm V_{app}/2$ at $z = 0, h$, where V_{app} is applied voltage, φ is the difference between the Fermi levels of the film and the electrode). Note that the amount of charge transfer between the FE and the electrode will depend on φ and no charge transfer will occur if $\varphi = 0$. Ideal metal electrodes are assumed whose work function is taken as that of Pt, a common electrode material (to determine electric BCs at the electrodes), and the polarization charges at the electrode interfaces are assumed to be completely screened, where we introduce image dipoles in the electrode with equivalent magnitude of the FE dipoles. For a state of zero depletion charge and $\lambda = \infty$, there is zero depolarizing field in the film. Temperature (T) dependent runs are carried out by varying T from 200 K to 1000 K, where the data in Figure 2 are used to introduce the T dependence of the E_F. The state obtained at the end of each iteration cycle is fed as the initial condition to the next T value similar to what indeed happens in an experimental measurement. This also sheds light on the point of SD-MD transition regardless of the randomness of the initial condition that the simulations start with.

III. RESULTS AND DISCUSSION

A. Simulation of an electroded n-type 40 nm PZT having high impurity density

We first analyze the effect of polarization on the electronic character (whether it is a Schottky or an Ohmic one) of metal-FE interfaces for relatively high impurity densities ($> 10^{26} m^{-3}$) in a 40 nm FE film. These phenomena in nanometer scale films, although an expected one, have started to stimulate interest for devices, where carrier transport through a junction could be switched on or off via manipulation of the polarization direction.[6,7,9,15] For a n-type impurity density of $10^{26} m^{-3}$ and a PZT film having a thickness of 40 nm sandwiched between metal electrodes at room temperature (RT) with the parameters provided in Table I, our solution prescribed in Sec. II gives the results plotted in Figure 3. n-type carrier accumulation occurs at the interface towards which the polarization points. During the computation, a question that arose was whether the charge accumulation at the interface to which the polarization vector points is due to
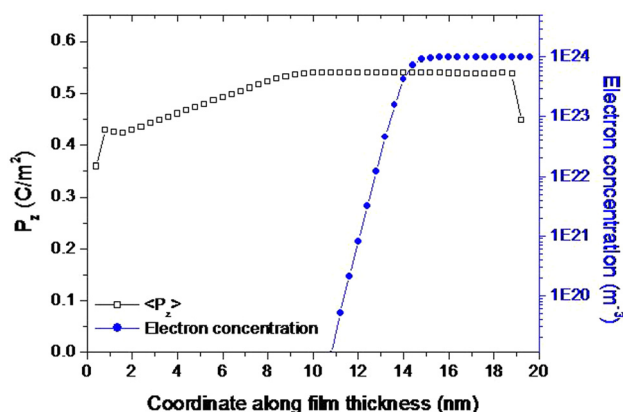
the presence of polarization or rather the "termination profile" of the P_z at that interface. For this reason, we solved Eqs. (1), (5), and (6) for $\lambda = 2$ nm and $\lambda = \infty$, where the latter implies that the surface behaves identical to the bulk. From Figure 3, it is clear that the polarization termination near the FE-electrode interface determines the extent of carrier accumulation, hence the electronic character. In the course of our study, we came across a study,[7] where the authors have arrived at similar results for BaTiO$_3$ (BT) sandwiched between SrRuO$_3$ (SR) on a SrTiO$_3$ (ST) substrate using atomistic first principles calculations. Using our approach and phenomenological parameters of BT retrieved from Ref. 50 and ideal electrode consideration, we get Figure 4(a). Figure 4(a) shows that our polarization profile obtained for 1.9×10^{27} m^{-3} n-type impurity density, misfit strain of -0.025 and a film thickness of $\sim$6 nm with a 0.4 V Schottky barrier height (the values used by Ref. 7) is in excellent agreement with the profile, these authors obtain for metal-oxide relative displacements; in addition, the polarization curve they generate by fitting parameters according to their work. The free electron distribution across the thickness we computed is also provided in Figure 4(b) and combined with the sign of the calculated electrostatic potential for this region (positive), clearly shows that the right FE-metal interface would behave as Ohmic-like. We find that ionized donors appear on the left handside and this interface is a
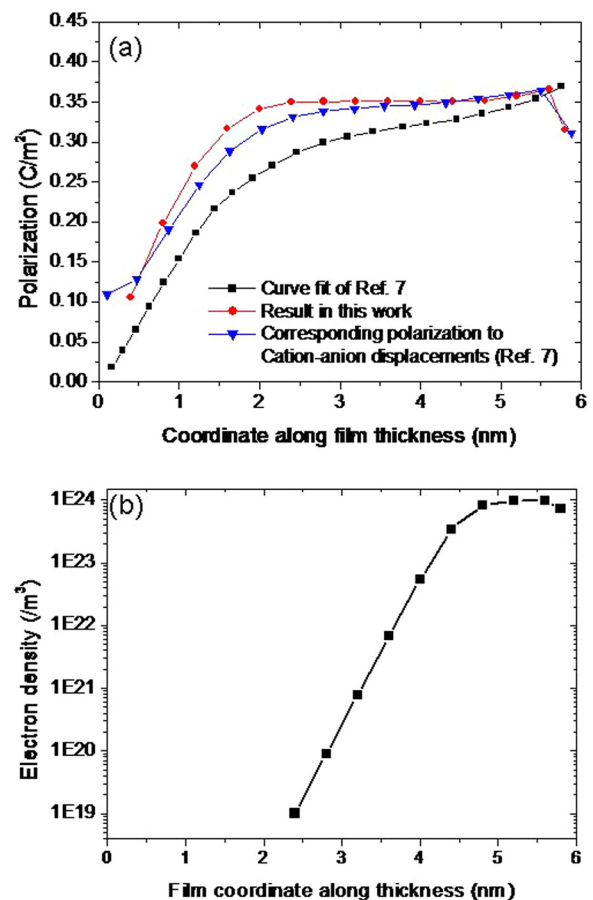
FIG. 4. (a) Comparison of our results obtained from thermodynamic theory with the first principles results of Ref. 7. (b) The electron distribution we computed for the same film using our approach.

FIG. 3. The polarization (P_z) profile and the electron density distribution in the 40 nm thick PZT film with 10^{26} impurity density.

Schottky one (not shown here). The authors of Ref. 7 probably choose to work with a rather high impurity density $(1.9 \times 10^{27}\,\mathrm{m}^{-3})$ to simulate carrier distribution in a film of about 6 nm thickness to be in the partial depletion regime as we find that 10^{25}–10^{26}/m^3 impurity densities, in the limit of full ionization, would put a 6 nm BaTiO$_3$ film into full depletion for a Schottky barrier height of 0.4 V (the value these authors take). Please note that we use, here, the atomistic first principles results for SR/BT/SR/ST in Ref. 7 to validate our approach and in the rest of our paper, we work with low-to-moderate impurity densities in thicker films. The main focus of our work is the thickness effect on the electronic character of the interface and the MD-SD stability and we show that carrier accumulation is possible at both interfaces if polarization termination near the interface leads to relatively large values of dP_z/dz for low-to-moderate impurity densities $(10^{20}$–$10^{24}\,\mathrm{m}^{-3})$. We also should emphasize that the polarization profile at low thickness (<10 nm) becomes rather insensitive to polarization BCs (for P_z), which we took into account using a value $\lambda = 2$ nm for SR/BT/SR/ST, if the ionized impurity density is very high ($> 10^{26}\,\mathrm{m}^{-3}$) and we kept such densities of impurities outside our scope in the following discussions.

B. Carrier profiles of films for various values of λ at RT

Following the important results that reveal the impact of λ on carrier distributions and electronic character of the FE-electrode interface, we extend our analysis to the case of 3 different values of λ: 0.4 nm, 2 nm, and 10000 nm (infinite), each of which generate lesser gradients of polarization near the interface, respectively, reminding that these values impose different "strengths" of ferroelectricity at the film surface. We consider the case of the 20, 40, and 80 nm films as these would have different charge distribution regimes for the densities of impurities considered. Of course, lower densities of impurities (such as $<10^{12}$/m^3) lead to a E_F closer to the middle of the bandgap and the aforementioned effect is less pronounced, leading to intrinsic behavior in all cases.

Our results for electron and hole distributions are in Figures 5(a)–5(f) to reveal the impact of λ in representative 20 nm, 40 nm, and 80 nm thick films when impurity density is $10^{24}\,\mathrm{m}^{-3}$. Films with $10^{20}\,\mathrm{m}^{-3}$ impurity density behave identical to the case of $10^{24}\,\mathrm{m}^{-3}$ for both small and large λ. Infinite values of λ cause full carrier depletion for the range of impurities, here, and does not lead to any interesting or different behaviors other than what we previously reported.[26,27,51] Figure 5 reveals that, in all cases, in this work, for $\lambda = 0.4$ nm and 2 nm, p-type carrier domination is observed despite the fact that the films are n-type FE: this is due to the depletion of the films of their electrons. That there is a possibility of a p-type Ohmic-like interface formation in a FE with n-type impurities is quite interesting for an interface potential barrier at the order of 0.7 eV for $\rho \cong 10^{24}\,\mathrm{m}^{-3}$ at RT, which is close to values in experiments for oxide FE–noble metal couples. Bringing the barrier height gradually to 0 eV (by raising the work function of the metal electrode to that of the E_F of the FE) causes the electrons to stay in and populate the film and density of holes go to zero, as

one would expect. In an opposite case, very high impurity densities would certainly eliminate any p-type behavior even for the barrier heights considered here as well as barrier heights measured in experiment. While thicker films behave so, the 20 nm film that always comes out to be in MD state for $\lambda = 0.4$ nm has nearly no electrons and relatively low concentrations of holes near the interfaces depending on the sign of local P_z owing to the fact that the electric fields are minimized due to electrical domain formation. In the SD state ($\lambda = 2$ nm), 20 nm film has some electron accumulation near the right interface owing to the relatively higher electric potential in this region (Figure 5(b)). 40 nm thick film appears to be favoring the MD state when $\lambda = 0.4$ nm for low-to-moderate impurity densities considered ($\leq 10^{24}\,\mathrm{m}^{-3}$). Unlike the 20 nm and 40 nm films, the 80 nm film is in SD state for $10^{16}\,\mathrm{m}^{-3}$, $10^{20}\,\mathrm{m}^{-3}$, and $10^{24}\,\mathrm{m}^{-3}$ impurity densities (See Table II) for all the λ values considered in this study. A small but finite electron density near the right interface exists for $\lambda = 2$ nm in the 80 nm film. For $\lambda = 0.4$ nm, the prominent carrier accumulation near the interfaces of the 80 nm film is due to steep gradients of P_z (Figure 5(e)). In the case of intrinsic FE film, the 40 and 80 nm structures also split into electrical domains when $\lambda = 0.4$ (see Figure 6) even in the limit of ideal electrodes. However, if we artificially grow the barrier height in the case of an intrinsic FE film, the films can sustain a stable SD state. Large barrier heights in a very similar system (PbTiO$_3$ with Pt electrodes) were claimed to be favoring a stable SD state down to a few nm film thickness.[52] Our finding, in the continuum limit, is due to depletion of electrons to equilibriate the Fermi levels, leaving a relatively high density of holes near one interface that generates a built in potential. Note that this is not expected to be a cause of possible asymmetry in hystereses as this hole accumulation at one of the interfaces will also depend on the sign of the applied potential.

From our results, it is clear that MD formation in relatively thin films (<40 nm) minimizes the electric fields near the interfaces and immediately leads to lower densities of carriers (both holes and electrons) with respect to what occurs in SD state. Thicker structures (80 nm) tend to exist in SD state for impurity densities $\geq 10^{16}\,\mathrm{m}^{-3}$ and carrier accumulation near interfaces is a strong function of the way polarization behaves in these regions. We must add here that, while λ is a parameter we control the interface polarization in our computational work, such effects can indeed be realized in experiments through the quality of the interface and local stoichiometry that could lead to dramatic weakening of the ferroelectricity at the interface and lead to carrier accumulation. Whether a SD or MD state might be expected especially for values of $\lambda < 1$ nm and low-to-moderate impurity densities is discussed in Sec. III C.

C. Thickness dependence of single domain stability at RT

As the carrier profiles, for the range of impurity densities we worked with, appear to be a strong function of film thickness particularly for strong suppression of ferroelectricity at the surfaces ($\lambda = 0.4$ nm), it is crucial to
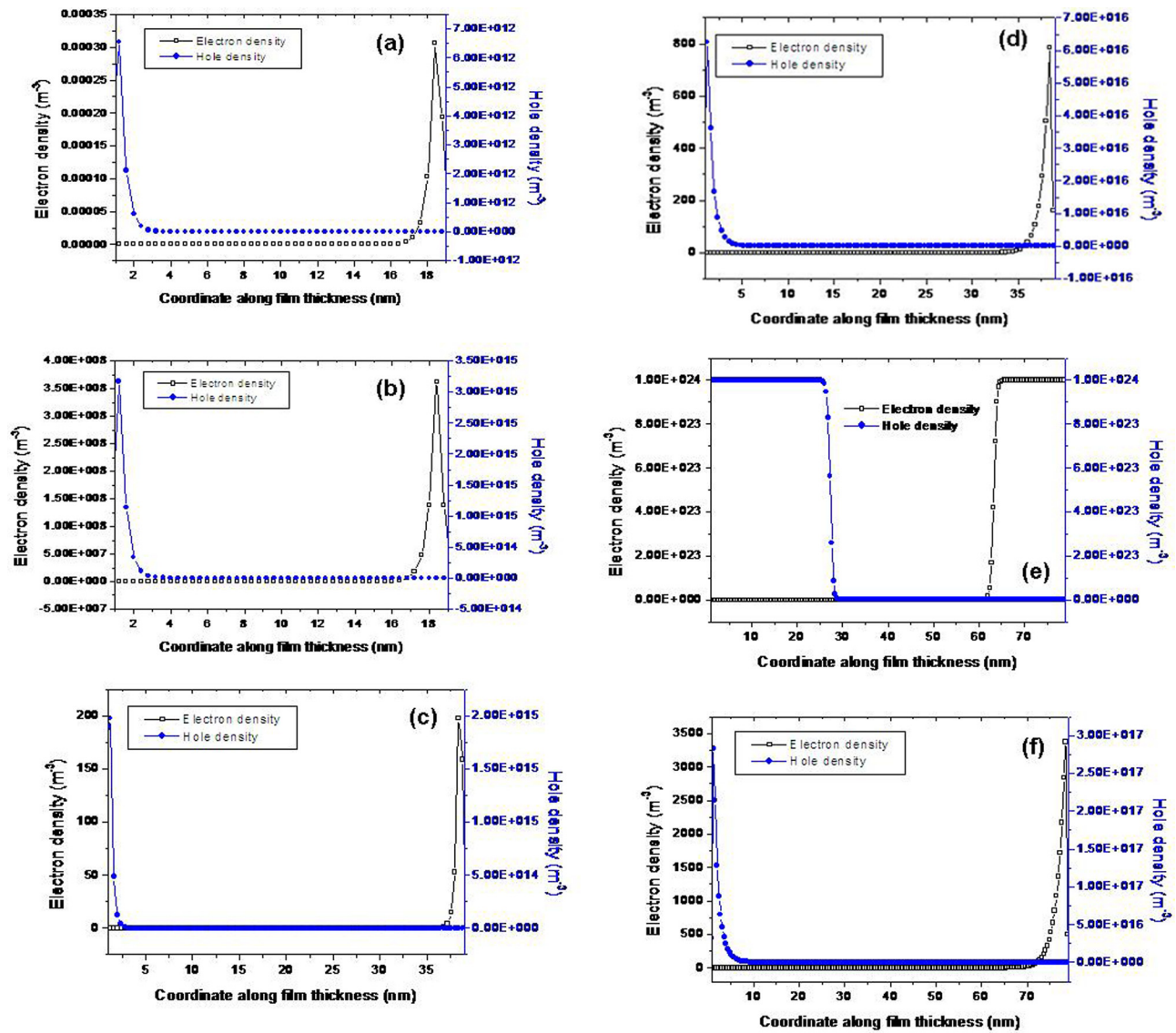
FIG. 5. The free carrier profiles for (a) the 20 nm thick film with $\lambda = 0.4$ nm and (b) $\lambda = 2$ nm, (c) the 40 nm film with $\lambda = 0.4$ nm and (d) the 80 nm film $\lambda = 2$ nm and (e) with $\lambda = 0.4$ nm and (f) $\lambda = 2$ nm. Please be reminded that the 20 nm and the 40 nm films are in MD state when $\lambda = 0.4$ nm and the profiles for these cases are taken along a domain with positive P_z. A similar but opposite carrier distribution occurs if we profile carrier density in a domain with negative P_z.

illustrate the SD stabilities as a function of film thickness. The thickness dependence of the SD stability for 4 different donor densities is examined: 10^{12} m^{-3}, 10^{16} m^{-3}, 10^{20} m^{-3}, and 10^{24} m^{-3}. For demonstrative purposes, 4 different thicknesses are considered: 20 nm, 40 nm, 60 nm, and 80 nm films, respectively, totaling the studied cases to 16 from which we deduce important trends and implications. For convenience, we give Table II to summarize the domain stability regimes of the films considered at RT for $\lambda = 0.4$ nm and after 3000 iterations. Relatively, large extrapolation lengths (>1–2 nm) only lead to hole accumulation at one of the interfaces depending on polarization sign as well as the barrier height as shown previously and no MD formation occurs for the range of impurities considered. For $\lambda > 1 - 2$ nm, MD states

TABLE II. Electrical domain stabilities in the 20, 40, 60, and 80 nm films for a metal work function of 5.5 eV. Note that the Fermi levels of the films depend on impurity concentrations, hence the barrier heights at the interfaces.

Impurity density (m^{-3})	80 nm film	60 nm film	40 nm film	20 nm film
10^{24}	Single domain	Single domain	Multi-domain	Multi-domain
10^{20}	Single domain	Single domain	Multi-domain	Multi-domain
10^{16}	Single domain	Single domain	Multi-domain	Multi-domain
10^{12}	Multi-domain	Multi-domain	Multi-domain	Multi-domain

can become stabilized only due to the finite screening effects of the electrodes (namely, presence of dead layers) as shown in previous works.[31,41]

The numerically computed polarization maps of some selected cases (from Table II) are given in Figure 6 when $\lambda = 0.4$ nm and $\lambda = 2$ nm, where the former leads to stronger suppression of ferroelectricity at the interface. The case of $\lambda = 2$ nm is given to demonstrate that SD state is stabilized for this value (also for $\lambda = 1$ nm but not shown here for brevity) in all films. We provide here the significant results only in order to avoid an overwhelming number of graphs that would make it hard to focus on the important outcomes. For 20 and 40 nm thickness, MD regime always comes out as the stable state regardless of the donor density and cannot be removed by low-to-moderate bias except domain wall motion when $\lambda = 0.4$ nm. Such a situation leads to weaker electric fields near the interface due to the alternating sign of polarization charges and sign of carriers (originating from impurities) to compensate polarization bound charges also follow this trend. Weak electric fields near the interface do not cause a significant carrier accumulation as was shown in Sec. III B. For 60 nm and 80 nm thick films, SD state appears to be possible for 10^{16}, 10^{20}, and 10^{24} m^{-3} donor densities (Only 10^{24} m^{-3} shown in Figure 6 for $\lambda = 0.4$ nm and 60 nm films) that are even lower than some experimental values

reported previously for such systems using C-V measurements and slope of the $1/C^2$ vs. applied bias plots.[53,54] 60 nm thick structure splits into electrical domains for 10^{12}/m^3 donor density or lower when $\lambda = 0.4$ nm as the interface region occupies a more significant volume of the film compared to the 80 nm thick structure in addition to the fact that the film has a stronger tendency to be fully depleted for the barrier heights in this work. The latter condition probably leaves insufficient density of electrons to neutralize the steep gradients of P_z near the interface for short λ. The 80 nm thick film, despite steep polarization gradients for $\lambda = 0.4$ nm, retains its SD state (not shown here) down to impurity densities of 10^{12} m^{-3} at which it starts to stabilize in MD form. We find that it is energetically more favorable to confine the carriers near the interfaces, where high values of potential appear in the case of thick films as long as the film is not close to "intrinsic." No such effect is observed in 20 or 40 nm films even for 10^{24} m^{-3} impurity density keeping in mind that the carrier density depends exponentially on local electrostatic potential (Eq. (2)). We conclude that accumulation of carriers near the interfaces can neutralize the local depolarizing fields emanating from steep polarization gradients and could stabilize a SD state especially in thick films (>40 nm in this work). This state can exhibit a hysteresis with applied electric field.
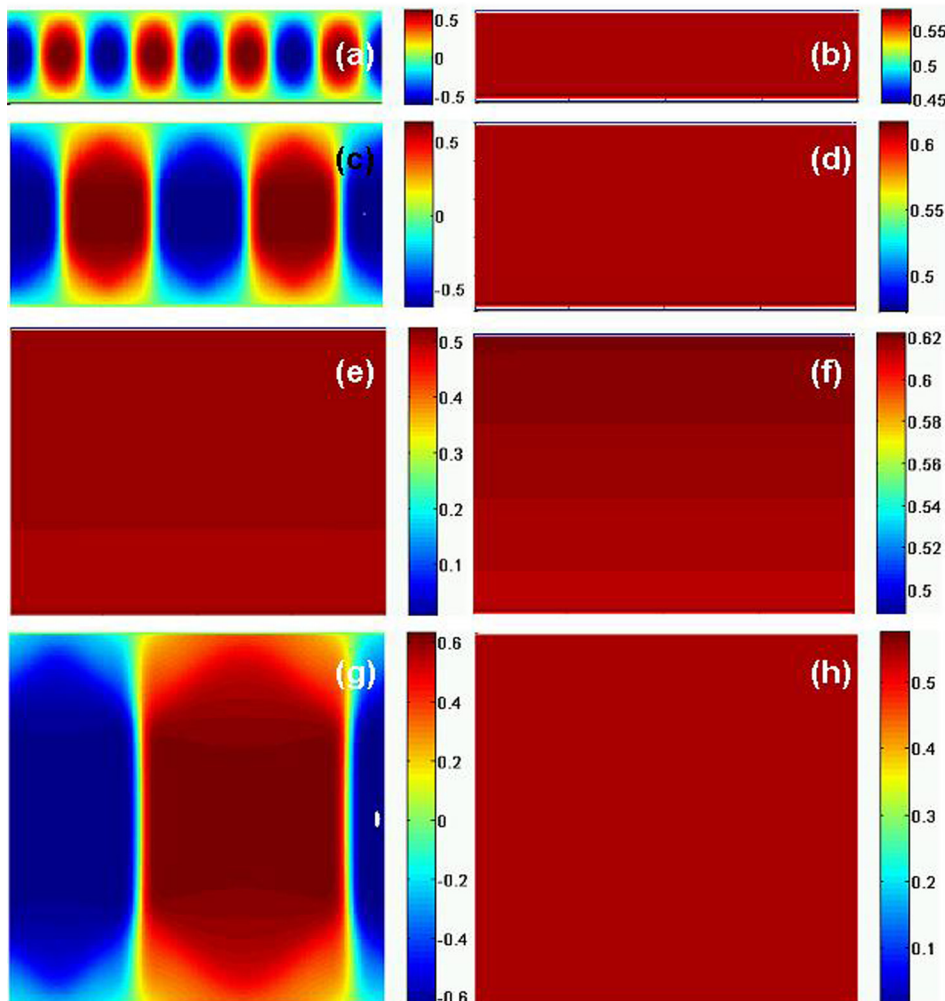
FIG. 6. P_z maps for 20 films with (a) $\lambda = 0.4$ nm and (b) $\lambda = 2$ nm, 40 nm films with (c) $\lambda = 0.4$ nm and (d) $\lambda = 2$ nm, 60 nm films with (e) $\lambda = 0.4$ nm and (f) $\lambda = 2$ nm and 80 nm films with (g) $\lambda = 0.4$ nm and (h) $\lambda = 2$ nm. Please note the difference in the scale legends of the $\lambda = 0.4$ nm and $\lambda = 2$ nm for films in SD state (due to the stronger depolarizing field effect in the case of $\lambda = 0.4$ nm).

D. Single domain-multi domain transition temperatures

We carried out cooling runs in the systems, we investigated for various impurity densities. In this manner, we could identify the range of temperatures, where the films remained in MD or SD state. The results are provided in Figure 7. We track $\langle|P_z(x,z)|\rangle$ and $\langle|P_x(x,z)|\rangle$, where we use
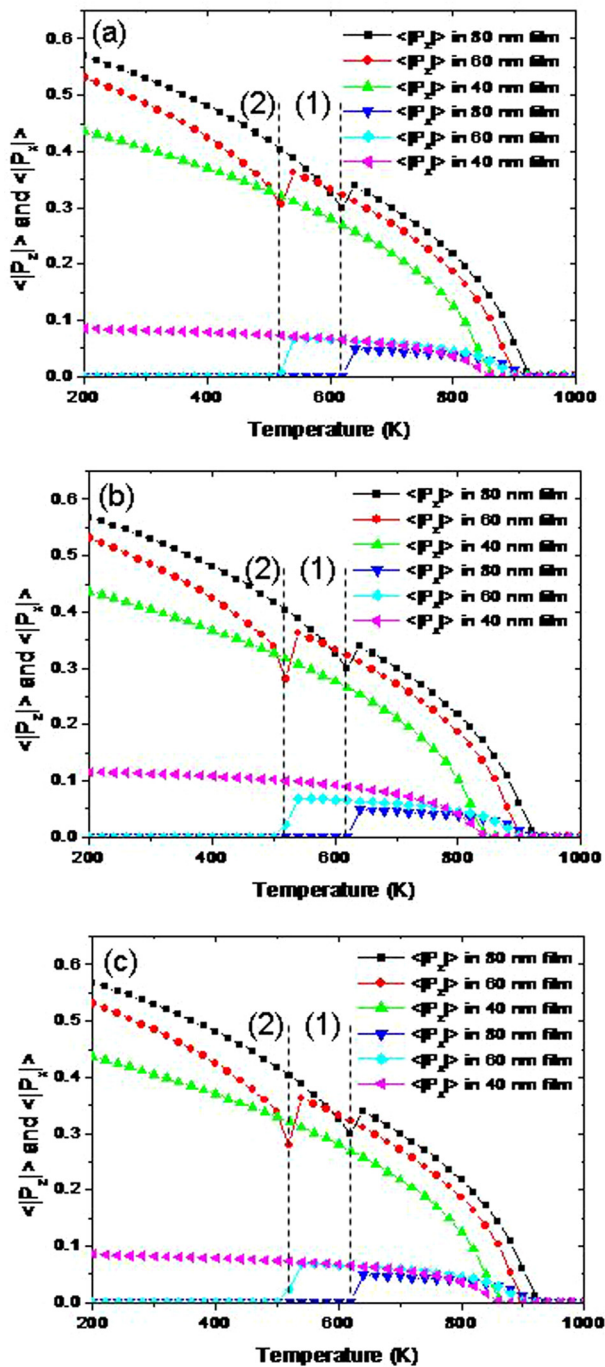
FIG. 7. $\langle|P_z|\rangle$ and $\langle|P_x|\rangle$ as a function of temperature to detect the Curie point and the MD-SD transition temperatures for (a) $10^{24}\,m^{-3}$ impurity density, (b) $10^{20}\,m^{-3}$ impurity density, and (c) $10^{16}\,m^{-3}$ impurity density. (1) and (2) denote the SD-MD transition in the 80 nm and 60 nm films, respectively. All plots are obtained for $\lambda = 0.4$ nm. The case when $\langle|P_x|\rangle$ goes to zero is the SD stability regime.

the latter to reveal the MD-SD transition in the films. The reason we do so is to ensure that we can detect the MD state unambigously as the regular average of P_z and P_x for the MD state is almost zero and goes undetectable. Although we did cooling runs for $\lambda = 2$ nm and $\lambda = 0.4$ nm, we focus on the latter as such values can stabilize the MD state in 20 nm and 40 nm films at all times for the range of impurities considered here as well as for low. It is important to note that T_C of the films is only a function of film thickness but not a strong function of impurity density for both small and large lambda. A similar note was made in the work of Bratkovsky and Levanyuk in their paper of year 2000.[55] For $\lambda = 2$ nm, electron depletion occurs in the entire film volumes (for low-to-moderate impurity densities) and SD state is retained in all cases. The SD stability here is related to reduce depolarizing fields due to λ being longer than the correlation length in these systems, which is presumed to be at the order of the unitcell length and this was concluded for FE films in the full insulator assumption.[38] We would like to remind that high impurity densities would lead to saw-tooth type domain structures as recently reported,[51] here, for large λ. In the current work, we do not go to high densities as we obtain the already published previous results[26,51] also for the metal/PZT/metal thin film capacitor considered here.

In the 60 nm and 80 nm films, strong suppression of ferroelectricity at the interfaces favors the MD state in the entire temperature range of ferroelectricity when the films are intrinsic or have low impurity densities ($\leq 10^{12}\,m^{-3}$). For $10^{24}/m^3$ impurity density, SD state persists below 520 and 620 K in 60 and 80 nm films, respectively, as also seen from $\langle|P_x|\rangle$ going to zero at the MD-SD transition shown in Figure 6: The SD state has only the P_z component as opposed to the MD state that does require P_x components to form closure domains near the interfaces. A similar picture is the case for $10^{20}/m^3$ in the 80 and 60 nm thick films (Figure 7(b)). Lower impurity densities (such as $10^{16}\,m^{-3}$, see Figure 6(c)) still appear to enforce the SD state in the 80 nm film but MD state starts to form in the 60 nm film when impurity density falls below $10^{16}/m^3$, a relatively low value (not shown here). The 20 and 40 nm structures are always in MD state and we give in Figure 7 only the 40 nm for brevity. Note that the presence of P_x in our work does not imply a strain induced monoclinic phase: we find that the stable phase in PZT for a misfit value of 1% compression is the tetragonal phase.

IV. CONCLUSIONS

Carrier distribution in a strained FE film with metallic ideal electrodes was studied as a function of film thickness and polarization BCs at the film surface. Ideal electrode approximation appears to work well as confirmed by the comparison of our results with that of Ref. 7. The FE was taken to be n-type contacting top-bottom electrodes having a work function greater than the E_F of the film, expected to give rise to Schottky junctions on both interfaces. The effect of carrier distribution on domain stabilities and possible SD-MD transition in a range of temperatures were also

examined. Thinner structures, when the surface polarization terminates with a strong gradient, are always in the MD regime regardless of the impurity densities considered including the intrinsic state. Thick structures (≥ 60 nm) can sustain a SD state even for relatively low impurity densities when the surface polarization has strong gradients (i.e., weak surface ferroelectricity). For λ having values of a few nanometers, all structures are in SD state as long as ideal electrodes are considered. We realized that, for weak surface ferroelectricity, thicker films are also in MD state but only at high temperatures near the Curie point. Strong gradients of polarization at the FE surface lead to carrier accumulation near these regions in relatively thick films and a SD state is favored. Growing the barrier height at the interfaces (by artificially raising the work function of the metal) could lead to SD states even in intrinsic films for steep surface polarization gradients and this is possibly due to depletion of the films of electrons and holes accumulate on one interface depending on sign of polarization that generates internal bias fields. For small barrier heights (<0.2 eV, for instance), intrinsic films in the case of weak surface ferroelectricity exist in MD state in order to confine the depolarizing fields near the interface. We also showed that sign of polarization controls the electron-rich and hole-rich regions but only when λ is at the order of a few nanometers or less. In films with very high impurity densities ($>10^{26}$ m^{-3}), the polarization profile becomes nearly insensitive to λ. The outcomes of our work imply the possible existence of Ohmic-like interfaces on both sides of an electroded FE depending on the type of the electrode and this is expected to enhance leakage currents. We also provided evidence that an n-type FE can behave like a p-type semiconductor for low-to-moderate impurity densities if the electrode work function is larger than that of the FE. Such a situation automatically generates an internal bias within the film, favoring P_z to be in a particular direction. Our results are important for understanding whether leakage can be interface driven or bulk controlled as many approaches formally consider carrier-depleted Schottky interfaces to occur in FE-metal contacts depending on the barrier height. The charge accumulation near or at the surfaces and related surface conductivities previously reported[56] could also be originating due to an effect similar to the one we report keeping in mind that electrical measurements are made via electrode contacts. We also became aware of another atomistic study, where depolarizing field in free standing BT films with top-bottom lattice termination plane asymmetry was also claimed to be a reason for charge transfer between O p states and Ti d states generating empty states for conduction, possibly stabilizing a polar FE state[57] and causing carrier accumulation at the interfaces but this is an intrinsic effect and is not a FE-electrode contact related occurrence. Finally, we realize that electrons expected to form a 2D gas at the electrode surface due to possible hole accumulation on the FE side could also be beneficial in optoelectronic devices tailoring surface plasmons. In an upcoming separate work, we intend to check the effect of finite screening length effects of the electrodes and how this phenomenon is altered due to polarization BCs at the FE film surface.

[1]H. Ishiwara, Curr. Appl. Phys. **9**, S2–S6 (2009).
[2]Y. Kaneko, Y. Nishitani, H. Tanaka, M. Ueda, Y. Kato, E. Tokumitsu, and E. Fujii, J. Appl. Phys. **110**, 084106 (2011)
[3]Y. Kaneko, H. Tanaka, M. Ueda, Y. Kato, and E. Fujii, IEEE Trans. Electron Devices **58**, 1311–1318 (2011).
[4]J. F. Scott, Jpn. J. Appl. Phys., Part 1 **38**, 2272–2274 (1999).
[5]S. Sakai and R. Ilangovan, IEEE Electron Device Lett. **25**, 369–371 (2004).
[6]D. Lee, S. H. Baek, T. H. Kim, J. G. Yoon, C. M. Folkman, C. B. Eom, and T. W. Noh, Phys. Rev. B **84**, 125305 (2011).
[7]X. H. Liu, Y. Wang, J. D. Burton, and E. Y. Tsymbal, Phys. Rev. B **88**, 165139 (2013).
[8]L. E. Stoflea, N. G. Apostol, C. Chirila, L. Trupina, R. Negrea, L. Pintilie, and C. M. Teodorescu, J. Mater. Sci. **49**, 3337–3351 (2014).
[9]I. Pintilie, C. M. Teodorescu, C. Ghica, C. Chirila, A. G. Boni, L. Hrib, I. Pasuk, R. Negrea, N. Apostol, and L. Pintilie, ACS Appl. Mater. Interfaces **6**, 2936–2939 (2014).
[10]H. Khassaf, G. A. Ibanescu, I. Pintilie, I. B. Misirlioglu, and L. Pintilie, Appl. Phys. Lett. **100**, 252903 (2012).
[11]L. Pintilie and M. Alexe, J. Appl. Phys. **98**, 123103 (2005).
[12]G. W. Pabst, L. W. Martin, Y. H. Chu, and R. Ramesh, Appl. Phys. Lett. **90**, 072902 (2007).
[13]L. Pintilie, I. Vrejoiu, D. Hesse, G. LeRhun, and M. Alexe, Phys. Rev. B **75**, 104103 (2007).
[14]M. A. Khan, T. P. Comyn, and A. J. Bell, Appl. Phys. Lett. **92**, 072908 (2008).
[15]L. M. Hrib, A. G. Boni, C. Chirila, I. Pasuk, I. Pintilie, and L. Pintilie, J. Appl. Phys. **113**, 214108 (2013).
[16]D. S. Jeong, R. Thomas, R. S. Katiyar, J. F. Scott, H. Kohlstedt, A. Petraru, and C. S. Hwang, Rep. Prog. Phys. **75**, 076592 (2012).
[17]G. Gerra, A. K. Tagantsev, and N. Setter, Phys. Rev. Lett. **98**, 207601 (2007).
[18]A. K. Tagantsev, G. Gerra, and N. Setter, Phys. Rev. B **77**, 174111 (2008).
[19]L. Pintilie, V. Stancu, L. Trupina, and I. Pintilie, Phys. Rev. B **82**, 085319 (2010).
[20]I. Pintilie, I. Pasuk, G. A. Ibanescu, R. Negrea, C. Chirila, E. Vasile, and L. Pintilie, J. Appl. Phys. **112**, 104103 (2012).
[21]I. B. Misirlioglu, M. B. Okatan, and S. P. Alpay, J. Appl. Phys. **108**, 034105 (2010).
[22]V. K. Yarmarkin, S. G. Shul'man, and V. V. Lemanov, Phys. Solid State **55**, 547–550 (2013).
[23]Y. Xiao, V. B. Shenoy, and K. Bhattacharya, Phys. Rev. Lett. **95**, 247603 (2005).
[24]V. B. Shenoy, Y. Xiao, and K. Bhattacharya, J. Appl. Phys. **111**, 084105 (2012).
[25]L. Yang and K. Dayal, Acta Mater. **60**, 6457–6463 (2012).
[26]I. B. Misirlioglu and M. Yildiz, J. Phys. D: Appl. Phys. **46**, 125301 (2013).
[27]I. B. Misirlioglu and M. Yildiz, J. Appl. Phys. **114**, 194101 (2013).
[28]A. N. Morozovska and E. A. Eliseev, J. Phys.: Condens. Matter **16**, 8937–8956 (2004).
[29]A. N. Morozovska and E. A. Eliseev, Phys. Rev. B **73**, 104440 (2006).
[30]A. N. Morozovska, E. A. Eliseev, S. V. Svechnikov, A. D. Krutov, V. Y. Shur, A. Y. Borisevich, P. Maksymovych, and S. V. Kalinin, Phys. Rev. B **81**, 205308 (2010).
[31]E. V. Chensky and V. V. Tarasenko, Zh. Eksp. Teor. Fiz. **83**, 1089–1099 (1982).
[32]Y. L. Li, S. Y. Hu, Z. K. Liu, and L. Q. Chen, Appl. Phys. Lett. **81**, 427–429 (2002).
[33]H. Chen, T. M. Cheng, S. Q. Chen, and T. C. Gang, Surf. Rev. Lett. **16**, 507–512 (2009).
[34]O. G. Vendik, S. P. Zubko, N. Y. Medvedeva, and Y. Natalia, J. Appl. Phys. **105**, 053515 (2009).
[35]A. P. Levanyuk and I. B. Misirlioglu, J. Appl. Phys. **110**, 114109 (2011).
[36]I. A. Luk'yanchuk, L. Lahoche, and A. Sene, Phys. Rev. Lett. **102**, 147601 (2009).
[37]W. A. Al-Saidi and A. M. Rappe, Phys. Rev. B **82**, 155304 (2010).
[38]M. D. Glinchuk, E. A. Eliseev, and V. A. Stephanovich, Phys. B: Condens. Matter **322**, 356–370 (2002).
[39]J. Junquera and P. Ghosez, Nature **422**, 506–509 (2003).

[40]N. Sai, A. M. Kolpak, and A. M. Rappe, Phys. Rev. B **72**, 020101 (2005).

[41]A. M. Bratkovsky and A. P. Levanyuk, Phys. Rev. Lett. **84**, 3177–3180 (2000).

[42]A. M. Bratkovsky and A. P. Levanyuk, J. Comput. Theor. Nanosci. **6**, 465–489 (2009).

[43]W. Zhong, R. D. Kingsmith, and D. Vanderbilt, Phys. Rev. Lett. **72**, 3618–3621 (1994).

[44]T. Kolodiazhnyi, M. Tachibana, H. Kawaji, J. Hwang, and E. Takayama-Muromachi, Phys. Rev. Lett. **104**, 147602 (2010).

[45]A. M. Bratkovsky and A. P. Levanyuk, Phys. Rev. Lett. **94**, 107601 (2005).

[46]R. Kretschmer and K. Binder, Phys. Rev. B **20**, 1065 (1979)

[47]J. Hlinka and P. Marton, Phys. Rev. B **74**, 104104 (2006).

[48]A. K. Tagantsev, Ferroelectrics **375**, 19–27 (2008).

[49]M. J. Haun, Z. Q. Zhuang, E. Furman, S. J. Jang, and L. E. Cross, Ferroelectrics **99**, 45–54 (1989).

[50]N. A. Pertsev, A. G. Zembilgotov, and A. K. Tagantsev, Phys. Rev. Lett. **80**, 1988–1991 (1998).

[51]I. B. Misirlioglu, H. N. Cologlu, and M. Yildiz, J. Appl. Phys. **111**, 064105 (2012).

[52]M. A. M. Polanco, I. Grinberg, A. M. Kolpak, S. V. Levchenko, C. Pynn, and A. M. Rappe, Phys. Rev. B **85**, 214107 (2012).

[53]C. P. A. K. Tagantsev, K. Brooks, and N. Setter, Integr. Ferroelectrics **4**, 1 (1994).

[54]L. Pintilie, I. Boerasu, M. J. M. Gomes, T. Zhao, R. Ramesh, and M. Alexe, J. Appl. Phys. **98**, 123104 (2005).

[55]A. M. Bratkovsky and A. P. Levanyuk, Phys. Rev. B **61**, 15042–15050 (2000).

[56]Y. Watanabe, M. Okano, and A. Masuda, Phys. Rev. Lett. **86**, 332–335 (2001).

[57]M. Krcmar and C. L. Fu, Phys. Rev. B **68**, 115404 (2003).